ANFIS_Parallelization_Control_on_Triple-Axis_Sun_Tracker_to_Minimize_Solar_Rays_Incidence_Angle_on_Photovoltaic

by Anfis_parallelization_control_on_triple-axis_sun_t
Anfis_parallelization_control_on_triple-axis_sun_t

Submission date: 17-Apr-2025 12:38PM (UTC+0700)
Submission ID: 2648738910
File name: acker_to_Minimize_Solar_Rays_Incidence_Angle_on_Photovoltaic.pdf (2.73M)
Word count: 11548
Character count: 60841

IEEE Access
Multidisciplinary | Rapid Review | Open Access Journal

Received 19 January 2025, accepted 8 February 2025, date of publication 14 February 2025, date of current version 20 February 2025.

Digital Object Identifier 10.1109/ACCESS.2025.3542337

RESEARCH ARTICLE

ANFIS Parallelization Control on Triple-Axis Sun Tracker to Minimize Solar Rays Incidence Angle on Photovoltaic

HARI ANNA LASTYA[1,2], (Student Member, IEEE), YUWALDI AWAY[1,3], (Member, IEEE), TARMIZI[3], (Member, IEEE), IRA DEVI SARA[3], (Member, IEEE), ROSLIDAR[3], (Member, IEEE), AND ANDRI NOVANDRI[4], (Student Member, IEEE)

[1]School of Engineering, Universitas Syiah Kuala, Banda Aceh 23111, Indonesia
[2]Universitas Islam Negeri Ar-Raniry, Banda Aceh 23111, Indonesia
[3]Department of Electrical and Computer Engineering, Universitas Syiah Kuala, Banda Aceh 23111, Indonesia
[4]Department of Computer Engineering, Universitas Serambi Mekkah, Banda Aceh 23249, Indonesia

Corresponding author: Yuwaldi Away (yuwaldi@usk.ac.id)

This work was supported by Lembaga Penelitian dan Pengabdian kepada Masyarakat (LPPM) of Universitas Syiah Kuala under Grant 168/UN11.2.1/PG.01.03/SPK/PTNBH/2024.

ABSTRACT This study proposes an Adaptive Neuro-Fuzzy Inference System (ANFIS) based on model with Parallelization Control Technique (PCT) implemented in a triple-axis sun tracker system. The system aims to maximize solar energy absorption by minimizing the angle of incidence of sunlight on Photovoltaic (PV) panels. It is designed with three manipulator arms, each controlled in parallel by a distinct ANFIS model. The primary goal is to adjust the PV panel orientation to optimal azimuth and altitude angles. The tetrahedron sensor is employed to detect the direction of sunlight. This study tests various types of consequent rules to find the optimal configuration for each ANFIS model, including first-order, second-order, and third-order polynomial functions. The analysis results show that the second-order consequent rule provides the highest accuracy across the three ANFIS models. The proposed system can cover azimuth range from 0° to 360° and altitude angle from 60° to 90°. The experiment also demonstrated that the system consistently moves toward a stable condition, even in the presence of minor disturbances. These findings indicate that ANFIS with PCT can minimize the angle of sunlight incidence, enhance system flexibility, and accelerate response time, making it a viable solution for increasing energy harvesting by PV panels.

INDEX TERMS ANFIS, parallelization control, photovoltaic, sun tracker, triple-axis.

I. INTRODUCTION

The sun tracker system is designed to automatically follow the sun's movement, maximizing sunlight reception on Photovoltaic (PV) panels [1]. This technology is essential in increasing energy production in PV systems, especially in areas with high sunlight intensity. PV efficiency heavily depends on the angle of sunlight incidence on the PV surface. The more optimal the angle, the greater the amount of sunlight absorbed, increasing the electrical energy produced [2], [3]. To maximize generated energy, the orientation of the panels needs to be adjusted in real-time so that the PV always maintains an optimal angle to the sunlight [4], [5], [6]. Conventional solar power plants are generally installed statically, so PV panels do not receive optimal sunlight exposure, especially in the morning and evening [7],. A sun tracker system can dynamically adjusted the PV orientation to remain perpendicular to the sunlight, thereby maximizing the electrical energy obtained [9], [10], [11]. Sun tracker systems have been discussed in several studies, including in [12], where a comparison between fixed PV systems and sun trackers was conducted. The results showed that sun trackers can increase electricity generation by 30% compared to fixed PV systems. Another study in [13] examined a sun tracker system

The associate editor coordinating the review of this manuscript and approving it for publication was Nasim Ullah.

using a Stewart platform mechanism, demonstrating that the sun tracker system can enhance energy generation by 32% compared to fixed PV systems. Additionally, [14] compares energy produced and consumed by sun tracker systems. The findings indicate that the total energy obtained from a sun tracker system is 26.9% higher than from a fixed PV system, with the energy consumption of the sun tracker reaching 5.63% or around 21.22 Wh and total energy production of 376.85 Wh. These studies show that sun trackers are superior to fixed PV systems. Furthermore, as discussed in [15], the popularity of sun tracker systems continues to rise along with the growing use of solar energy as an alternative energy source. Further developments in sun tracker systems cover various aspects, including manual control through internet networks as studied in [16] and [17], bluetooth-based control as examined in [18], and automatic control using solar trajectory models as explored in [19] and [20].

In its implementation, a sun tracker requires an effective sensor to accurately detect the sun's position coordinates. This study proposes a type of sensor called a tetrahedron sensor. The survey of the tetrahedron sensor was first introduced in [21], which analyzed the design and structure of the sensor, consisting of three photoresistors. The study's results demonstrated that the tetrahedron sensor could detect the sun's position with a maximum wide Field of View (FOV) of 289.4° and an accuracy of ±1.67°. Further research on the tetrahedron sensor is discussed in [22], which focuses on developing a sensor based on phototransistors to replace photoresistors. Additionally, [23] examined the effect of the tetrahedron sensor's dimensions on the sun tracker's performance in tracking the sun's position. The results showed that increasing the height of the tetrahedron correlates with an increase in FOV, where a tetrahedron with a height of 4.5 cm has an FOV of 289.4°, while a height of 10.2 cm reaches an FOV of 310°.

An appropriate control algorithm and drive mechanism are needed to control the orientation movement of a sun tracker. The control algorithm is necessary to quickly and stably adjust the panel position, reducing energy losses caused by suboptimal angles of incidence. Meanwhile, the drive mechanism is required to support smooth and precise movements. Several studies have examined single-axis and dual-axis drive mechanisms with various algorithms, as shown in Table 1. Based on these studies, the design of the control mechanism in a sun tracker significantly influences the system's response time in following the sun's movement. On the other hand, some studies have developed triple-axis drive mechanisms. This mechanism is designed to improve the vertical orientation adjustment of PV panels. In [24], it is stated that the efficiency of commercial PV typically ranges from 10-20%. Applying a triple-axis mechanism to the sun tracker increases PV efficiency by up to 25%. In [25], it is revealed that the power output generated by PV on a triple-axis sun tracker is 19% greater than that of a dual-axis mechanism. This improvement is due to the triple-axis mechanism's ability to adjust the PV panel's height, enabling it to prevent shadows from surrounding objects from falling onto the panel surface. Furthermore, [26] states that a triple-axis sun tracker can be implemented on a mobile platform, allowing the panel to adjust its orientation to maintain an optimal position even if the platform moves. Although triple-axis sun trackers have significant potential for improving PV efficiency, there are still technical challenges in determining a control method to optimize panel orientation. With the proper control method, the system can adapt to changes in the sun's position and avoid shadows from objects falling on the panel surface [27]. One approach capable of adapting to changing conditions is the Adaptive Neuro-Fuzzy Inference System (ANFIS).

ANFIS is an algorithm that combines approaches from Artificial Neural Networks (ANN) and Fuzzy Inference Systems (FIS) to model complex relationships between inputs and outputs [28]. FIS handles uncertain data using fuzzy rules and membership functions to map input values into fuzzy sets [29]. Meanwhile, ANN is responsible for the learning process, where parameters within the fuzzy system, such as membership functions and fuzzy rules, are automatically optimized based on the provided training data [30]. The main processes in ANFIS include fuzzification, which transforms input values into fuzzy values; fuzzy inference, which generates fuzzy output based on fuzzy rules; and defuzzification, which converts the fuzzy output into a numerical value [31], [32]. Several studies have explored the application of ANFIS in various fields. For example, in [33], ANFIS was applied to model machine behaviour in a gas turbine by estimating its operational parameters and improving its performance and durability. Furthermore, [34] discusses the application of ANFIS for controlling dynamic force and position in a Programmable Universal Machine for Assembly (PUMA) robot. Another study [35], applied ANFIS to model the behaviour of an air spring system, which was used to control the solenoid valve of the air spring system to reduce mass acceleration. In addition, other studies have discussed the application of ANFIS in controlling sun trackers. For instance, [36] compared the performance of a Proportional Integral Derivative (PID) controller with ANFIS, with both algorithms optimized using the Firefly Algorithm (FA) to enhance system speed and stability. The findings showed that the ANFIS-FA combination significantly reduced overshoot and accelerated settling time. Furthermore, [37] explored the ANFIS application by comparing single-axis and dual-axis sun tracker mechanisms, concluding that ANFIS with five membership functions was more optimal in controlling both sun tracker mechanisms, yielding high prediction accuracy and low error. Additionally, [38] conducted further analysis on ANFIS as a sun tracker controller, examining the effect of the number of membership functions on model training. This study revealed that the number of membership functions directly affects model performance, with an increase in membership functions leading to reduced error. Moreover, ANFIS offers the flexibility of fuzzy logic, enabling it to

TABLE 1. Literature review of control mechanism on sun tracker.

Paper	Year	Algorithm	Control Mechanism	Rise Time (s)	%Error
Yuwaldi Away et al. [44]	2023	PID-ANN	Dual-Axis	2.18	1.75%
Andri Novandri et al. [45]	2022	PID	Dual-Axis	1.85	2.6%
Fitri Rahmah et al. [46]	2022	Fuzzy-PD	Single-Axis	7.43	0.43%
Baisrum et al. [47]	2021	ANFIS	Single-Axis	-	1.25%
Imam Abadi et al. [48]	2020	Fuzzy-PID	Dual-Axis	8.2	-
Jalal Farazi et al. [49]	2020	PO-ANN	Dual-Axis	0.94	-
Zubairu A. Yusuf et al. [50]	2019	ABC	Single-Axis	2.37	-
Bamigboye O. Oladayo et al. [51]	2016	IMC-PID	Dual-Axis	1.78	-
Mirza Muhammad Sabir et al. [52]	2016	PID	Dual-Axis	2.2	0.5%

learn from data and automatically adjust parameters [39]. The implementation of ANFIS is less complex compared to other control methods, such as Linear Quadratic Regression (LQR) and Model Predictive Control (MPC). MPC has significantly higher complexity than ANFIS, as it requires solving optimization problems at each time step to determine the optimal control signal [40]. Additionally, LQR has low complexity because it only requires solving a functional quadratic equation. However, LQR is not designed to handle nonlinear systems, such as a triple-axis sun tracker [41]. Meanwhile, the ANFIS approach, which is a hybrid algorithm combining ANN and FIS, can quickly adjust parameters. This makes it highly suitable for real-time systems that demand quick responses and the ability to maintain responsiveness to environmental changes [42], [43]. Based on these studies, it is concluded that the ANFIS model can improve control performance in sun tracker systems, especially with additional optimization or increased membership functions. This makes ANFIS a practical approach for controlling PV panel orientation.

Based on these studies, most current sun tracker systems still rely on single-axis or dual-axis mechanisms, which have limitations in vertical adjustments and in avoiding shadows from objects surrounding the panels. On the other hand, research on triple-axis mechanisms is still minimal. Additionally, optimization techniques are needed to enhance the performance of the ANFIS algorithm in managing the complexity of sun tracker systems, particularly in triple-axis mechanisms. As a solution, the sun tracker system with a triple-axis drive mechanism is proposed. This proposed mechanism uses three manipulator arms, each driven by a servo motor. These three arms adjust the PV panel orientation along three axes, allowing the sun tracker to control movement at azimuth and altitude angles. A tetrahedron sensor consisting of three phototransistors arranged on each side of the tetrahedron, detects the sun's position. Additional optimization of the ANFIS algorithm is proposed to control the servo motors by applying the Parallelization Control Technique (PCT). This control method aims to divide computational processes into parts that can be executed in parallel, thereby enhancing computational efficiency and processing speed, especially in complex tasks. PCT enables multiple control processes to run simultaneously, reducing latency and improving system responsiveness. ANFIS-PCT offers an optimal balance between computational complexity, robustness against nonlinearity, and real-time responsiveness, making it the best solution for triple-axis sun tracker systems. In this proposed sun tracker, the system is divided into three processes that are responsible for controlling each servo motor's rotation angle. Input data is obtained from the tetrahedron sensor readings, with input variables varying for each process, resulting in distinct ANFIS models. ANFIS modelling is conducted by designing the network structure, determining the membership functions, and establishing fuzzy rules. Within the fuzzy rules is a consequent rule, part of the fuzzy rule that defines the output based on the fulfilled input conditions. An analysis of the consequent rules is necessary to achieve an optimal model. This study examines three types of consequent rules to identify the most optimal model. The three types of proposed consequent rules are polynomial functions of first-order, second-order, and third-order. Each of these orders has different complexity and mapping capabilities in identifying the relationship between inputs and outputs, requiring evaluation to determine the most suitable model for the sun tracker. This research focuses on minimizing the solar incidence angle to enhance the electrical energy production of PV systems. When the solar incidence angle on the panel surface approaches zero, the amount of sunlight absorbed by the PV reaches its maximum, directly increasing the generated electrical output.

The novelty of this research lies in the implementation of PCT in ANFIS, which enables the division of computational processes into multiple parts running concurrently. Additionally, this study analyzes various consequent rule configurations in the ANFIS model, including first-order, second-order, and third-order polynomial functions, to determine the most optimal configuration. The main contributions of this paper are as follows:

- We propose a sun tracker system using a triple-axis mechanism consisting of three manipulator arms to control the azimuth and altitude angles. This system enables

PV panels to adjust their angles optimally to the direction of incoming sunlight.
- We propose an ANFIS algorithm with PCT to control the movement of the sun tracker through separate control processes, making the system more responsive and accurate.
- We demonstrate that the second-order consequent rule provides the best performance in controlling the sun tracker, effectively minimizing the angle of incoming sunlight on the PV panel.

For convenience, the abbreviations used in this paper are summarized in Table 2.

TABLE 2. Summary of abbreviations.

Abbreviation	Meaning
ANFIS	Adaptive Neuro-Fuzzy Inference System
ANN	Artificial Neural Networks
CV	Coefficient of Variation
FIS	Fuzzy Inference Systems
LSE	Least Squares Estimation
MAE	Mean Absolute Error
MAPE	Mean Absolute Percentage Error
PCT	Parallelization Control Technique
PID	Proportional Integral Derivative
PV	Photovoltaic
RMSE	Root Mean Squared Error

II. MATERIAL AND METHODS

A. TETRAHEDRON SENSOR

The tetrahedron sensor is a type of sensor used to detect the position of sunlight. This sensor has a pyramid shape with three sides, each equipped with a light sensor in the form of a phototransistor. Figure 1 shows a phototransistor in the center of each side of the pyramid, with each position labelled P_1, P_2, and P_3. The sensor has a height of 10 cm and a base length of 5 cm. The type of light sensor and the dimensions of the tetrahedron are based on previous studies [22], [23]. The tetrahedron sensor operates on the principle of comparing values from each phototransistor. Based on these comparisons, the sensor can determine the sun's position regarding azimuth and altitude.

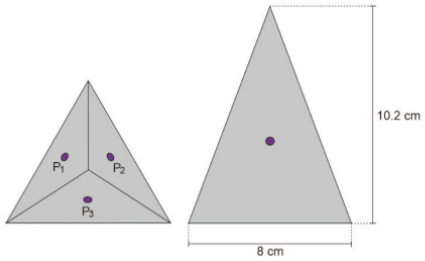

FIGURE 1. Tetrahedron sensor.

B. ADAPTIVE NEURO-FUZZY INFERENCE SYSTEM

ANFIS is a hybrid intelligent system that combines the strengths of fuzzy logic and ANN. Fuzzy logic provides a reasoning approach that mimics human thinking and can handle uncertainty and ambiguity. At the same time, ANN can learn from data and recognize complex patterns [53], [54]. The ANFIS architecture consists of several layers, each responsible for specific operations. The first layer performs fuzzification, where membership functions map input values to fuzzy sets. The second layer is the rule layer, where the firing strength of fuzzy rules is calculated. The third layer normalizes the firing strengths, while the fourth layer generates the output by multiplying the normalized firing strength with the consequent part of the fuzzy rules. Finally, the output layer combines these results to produce the final output [55].

ANFIS is trained to optimize fuzzy parameters through a learning method that combines the concepts of ANN and fuzzy. The training starts by determining the initial structure of ANFIS, including fuzzy rules, membership functions, and rule types [56]. Training data guides the training process, where the system updates the membership function and consequent parameters [57]. The training process typically consists of two phases: forward pass and backward pass. In the first process, the forward pass, input is fed into ANFIS, and the output is computed through the fuzzy inference mechanism, including fuzzification, firing strength calculation, normalization, and defuzzification to produce the final output [58]. The proposed ANFIS network structure in this study is shown in Figure 2. The first layer is the fuzzification layer, where each node in this layer calculates the membership degree of each input based on the corresponding membership function. The membership function of each input can be calculated using the following equation [59],

$$\mu_j(x_i) = f_j(x_i) \tag{1}$$

where, $\mu_j(x_i)$ is the membership degree for input x_i in the fuzzy set j and $f_j(x_i)$ is the membership function of input x_i in the fuzzy set j. In this study, a Gaussian Membership Function is used, which is expressed in the following equation,

$$f(x) = gaussian(x; c, \sigma) = e^{-\frac{1}{2}\left(\frac{x-c}{\sigma}\right)^2} \tag{2}$$

where, c is the mean value that serves as the center of the membership function, and σ is the standard deviation that determines the width of the membership function.

The second layer is the rule layer, where each node represents the firing strength for each fuzzy rule formed based on the combination of membership functions for each input. The firing strength is calculated as the product of the input signals that represent the premises in the fuzzy rules, as expressed in

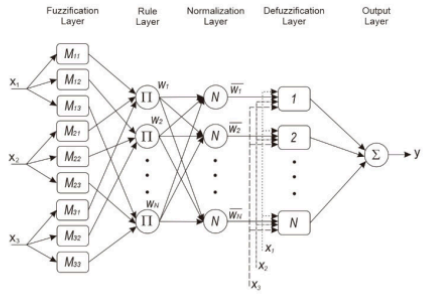

FIGURE 2. The architecture of ANFIS network.

the following equation,

$$w_i = \prod_{i=1}^{3} \mu_j (x_i) \tag{3}$$

where, w_i represents the output firing strength for rule i. Then, the firing strength values are normalized in the third layer, the normalization layer. This process ensures that the relative contribution of each fuzzy rule is correctly accounted for so that the total firing strength of all rules equals 1. The normalization process is performed using the following equation,

$$\overline{w_i} = \frac{w_i}{\sum_{i=1}^{N} w_i} \tag{4}$$

where, $\overline{w_i}$ represents the normalized firing strength and N is the number of fuzzy rules. Next, in the fourth layer, the defuzzification layer, each node multiplies the normalized firing strength by the output of the consequent fuzzy rule using the following equation,

$$z_i = \overline{w_i} \, . f \, (x_i) \tag{5}$$

where, z_i represents the defuzzified output for input x_i and $f\,(x_i)$ represents the output of the consequent rule for rule i. The consequent rule is a mathematical expression that determines the fuzzy output based on the input and the existing rules.

Next, in the fifth layer is the output layer. In this layer, each node combines all the signals received from the previous layers to produce the final output of the ANFIS, as expressed by the following equation,

$$y = \sum_{i=1}^{N} z_i \tag{6}$$

The consequent parameters are updated using the Least Squares Estimation (LSE) method by calculating the error between the system output y and the target output y_t, based on the total dataset m. The error is defined as follows,

$$E = \frac{1}{2} \sum_{i=1}^{m} (y_i - y_{t,i})^2 \tag{7}$$

After that, in the second process, the backward pass is performed using the backpropagation method to minimize the error by updating the parameters c and σ of the membership function based on the calculated error. To update the parameter c, the following equation is used,

$$c_{new} = c_{old} - \eta \frac{\partial E}{\partial c} \tag{8}$$

where, $\frac{\partial E}{\partial c}$ is the partial derivative of the error concerning c and η is the learning rate. Then, to update the parameter σ, the following equation is used,

$$\sigma_{new} = \sigma_{old} - \eta \frac{\partial E}{\partial \sigma} \tag{9}$$

where, $\frac{\partial E}{\partial \sigma}$ is the partial derivative of the error concerning σ. This process is repeated until the error reaches a minimum value or until a certain number of iterations is reached.

C. SUN TRACKER SYSTEM

Figure 3 shows the physical device of the sun tracker system. The proposed design implements a triple-axis mechanism with three manipulator arms. This mechanism allows the system to follow the sun's position more quickly as the motors move in parallel. The system uses servo motors as its actuators.

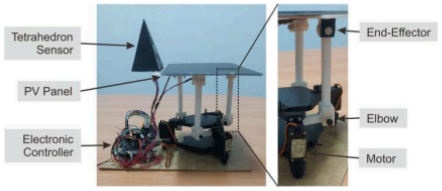

FIGURE 3. Proposed triple-axis sun tracker.

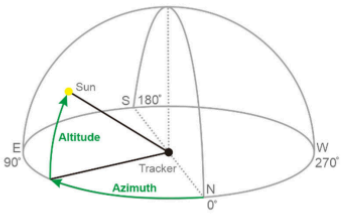

FIGURE 4. The movement of sun's position.

In the testing process, the sun tracker system is compared with the sun's movement path to evaluate the performance of

the proposed system. Figure 4 illustrates the position of the sun relative to the tracker. Two main parameters are used to determine the sun's position: azimuth and altitude. Azimuth is the horizontal angle measured clockwise from the north. An angle of 90° means the sun is in the east, 180° in the south, and 270° in the west. Azimuth indicates the sun's direction along the horizon [60]. Meanwhile, altitude measures the sun's height above the horizon, calculated from the horizontal line to the sun's position. This angle changes throughout the day, starting at 0° when the sun rises, reaching its peak at noon, and then returning to 0° when the sun sets [61]. The sun's movement path can be calculated using astronomical formulas based on location and time. The equation to calculate the solar azimuth angle (ϕ_S) is expressed as follows,

$$\sin \phi_S = \frac{\cos \delta \ . \ \sin \gamma_H}{\cos \varphi_S} \tag{10}$$

where, δ is the solar declination angle, which can be calculated using the following equation,

$$\delta = 23.45^\circ \ . \ \sin\left(360 \ . \ \frac{284 + n}{365}\right) \tag{11}$$

where, n is the day number in the year. Meanwhile, γ_H is the solar hour angle, expressed as follows,

$$\gamma_H = 15^\circ \ (T_r - 12) \tag{12}$$

where, T_r is the true time, ranging from 0 to 24 hours. Then, φ_S is the solar altitude angle, expressed as follows,

$$\sin \varphi_S = \sin \omega \ . \ \sin \delta + \cos \omega \ . \ \cos \delta \ . \ \cos \gamma_H \tag{13}$$

where, ω represents the latitude coordinate based on the location on earth.

III. PROPOSED METHOD

The proposed method includes ANFIS modelling and determining the most optimal consequent rule to be applied. It also explains the proposed mechanical structure in the sun tracker system, which aims to optimize the movement of the solar panels to enhance solar energy absorption efficiency. The modeling process of ANFIS and the simulation of the sun tracker system were conducted on a computer with an AMD Ryzen 5 4600H CPU, 16 GB DDR4 RAM, and an NVIDIA GeForce GTX 1650 Ti GPU with 4 GB memory. Additionally, the software used includes Python 3.10 with TensorFlow version 2.12.0. The flowchart illustrating the entire proposed system, including the ANFIS modeling method and sun tracker control, is shown in Figure 5.

A. ANFIS MODEL

In this study, ANFIS is used to control the movement of servo motors based on the light intensity readings from the tetrahedron sensor. The rotation of the motors affects the movement of the manipulator arms, which direct the PV towards the sun. This study proposes ANFIS-PCT, consisting of three ANFIS models, each responsible for controlling a different motor, as shown in Figure 6, with the structure of each network shown in Table 3. The proposed membership function utilizes a Gaussian function chosen for its flexibility in modeling nonlinear relationships between inputs and outputs [62]. The number of membership functions for each input was determined based on performance evaluation through simulation, where three membership functions per input demonstrated a balance between computational complexity and model accuracy. Using more than three membership functions increases accuracy but significantly adds to computation time, making it unsuitable for real-time sun tracker systems. The learning rate parameter was set to 0.01 after testing, which showed that this value provides stable convergence without compromising training speed. Additionally, the number of training iterations was set to 5000 epochs based on observations indicating that the model achieves minimum error performance within this range.

TABLE 3. Proposed ANFIS structure.

Parameter	Value	Description
Number of input	3	Number of nodes in the input layer
Number of output	1	Number of nodes in the output layer
Number of fuzzy MF 1	3	Number of membership functions at input node 1
Number of fuzzy MF 2	3	Number of membership functions at input node 2
Number of fuzzy MF 3	3	Number of membership functions at input node 3
Membership function	Gaussian function	Membership function at input
Number of rules	27	Number of rules fuzzy
Number of datasets	1945	Number of data for training process
Learning rate	0.01	ANFIS learning rate parameter

Based on Figure 6, ANFIS 1 model controls the angle (θ) of servo motor 1 based on inputs from P_1 sensor, P_2 sensor, and the initial angle (θ_0) of servo motor 1. ANFIS 2 model controls the angle of servo motor 2 based on inputs from P_2 sensor, P_3 sensor, and the initial angle of servo motor 2. Meanwhile, ANFIS 3 model controls the angle of servo motor 3 based on inputs from P_3 sensor, P_1 sensor , and the initial angle of servo motor 3. Next, the output angle of each motor is calculated and used to move the three arms of the sun tracker.

There is a consequent rule in defuzzification, obtaining results based on fuzzy rules by describing the mathematical relationship between input and output [63]. The parameters in the consequent rule are optimized during the training process to ensure that the model can accurately predict the output based on the given data. This paper proposes three types of consequent rules: polynomial functions of first-order, second-order, and third-order. These consequent rules are applied to

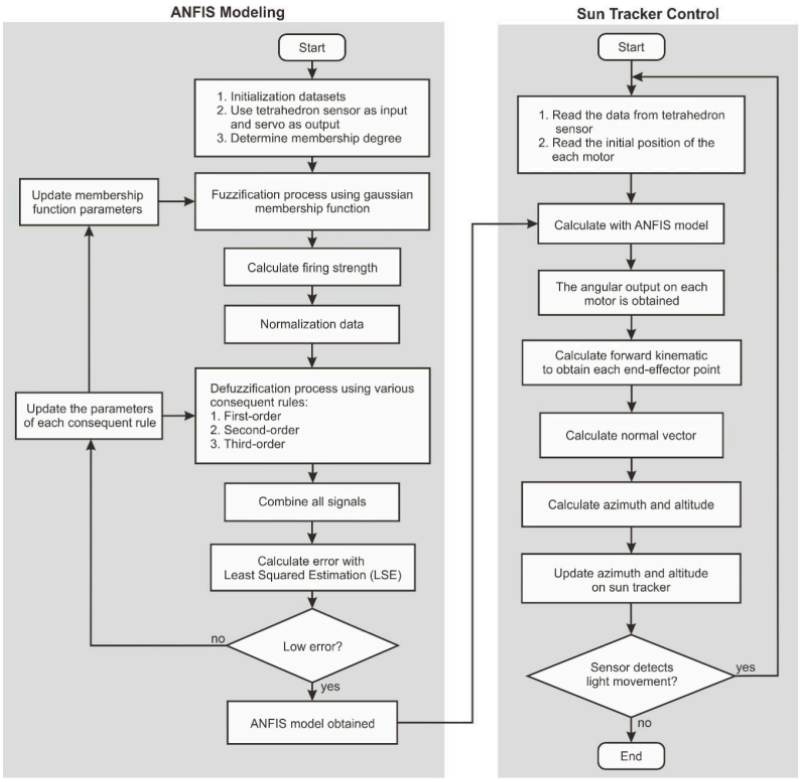

FIGURE 5. Flowchart of ANFIS modeling and solar tracking control system.

Eq. (5). The first-order function is expressed as follows,

$$f(x_i) = \sum_{i=1}^{3} p_i x_i + r \tag{14}$$

where, $f(x_i)$ represents the output of the consequent rule. p_i is the first-order parameter for input x_i, and r is the bias constant of the rule. Meanwhile, for the second-order function, the equation is as follows,

$$f(x_i) = \sum_{i=1}^{3} p_i x_i + \sum_{i=1}^{3} q_i x_i^2 + \sum_{1 \leqslant i < k \leqslant 3} c_{i,k} x_i x_k + r \tag{15}$$

where, q_i is the second-order parameter for input x_i and $c_{i,k}$ is the parameter for the cross terms between inputs x_i and x_k.

Then, for the third-order function, the equation is as follows,

$$f(x_i) = \sum_{i=1}^{3} p_i x_i + \sum_{i=1}^{3} q_i x_i^2 + \sum_{1 \leqslant i < k \leqslant 3} c_{i,k} x_i x_k + \sum_{i=1}^{3} t_i x_i^3 + r \tag{16}$$

where, t_i is the second-order parameter for input x_i.

B. MECHANICAL STRUCTURE OF SUN TRACKER

This sun tracker system configuration uses three manipulator arms, as shown in Figure 7. The model of the manipulator arms is arranged in a parallel configuration, with servo motors as the actuators. These three arms are connected to a triangular plane that serves as the base for the PV. Points J_1, J_2, and J_3 connect the plane to the manipulator arms. The height of

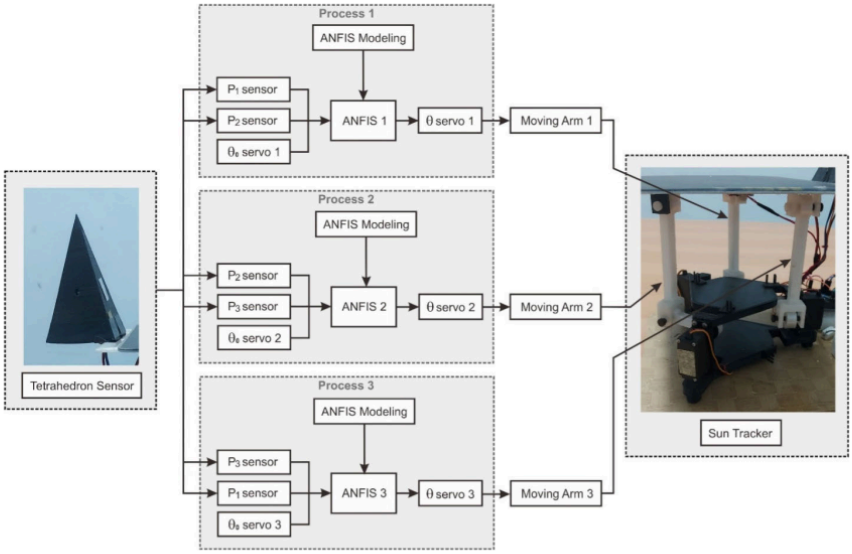

FIGURE 6. Block diagram of proposed tracker system with ANFIS-PCT.

these points will affect the orientation of the PV in following the sun's movement.

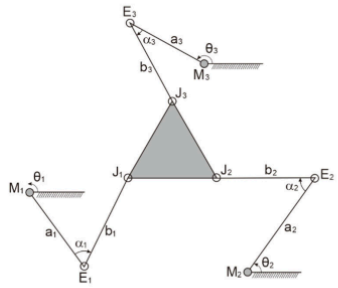

FIGURE 7. Triple-arm manipulator configuration on sun tracker system.

The configuration of the manipulator arm is shown in Figure 8(a). The arm consists of the upper arm (b_i) and the lower arm (a_i), with lengths of 3.7 cm and 1.6 cm, respectively. Additionally, there are two connection points: the elbow point (E_i) and the end-effector point (J_i), as well as a drive point M_i as the motor (for $i = 1, 2, 3$). The E_i point is the connection between the lower and upper arm, while J_i is the connection between the upper arm and the base plane where the PV is mounted. Figure 8(b) shows the drive mechanism of the manipulator arm. The angle β_i is the orientation angle of the manipulator arm relative to the x-axis. The movement of motor M_i will create an angle θ_i. This angle will affect the value of angle α_i at point E_i, causing the coordinates at point J_i to change. These coordinate changes can be calculated using the following forward kinematic equation [64], [65],

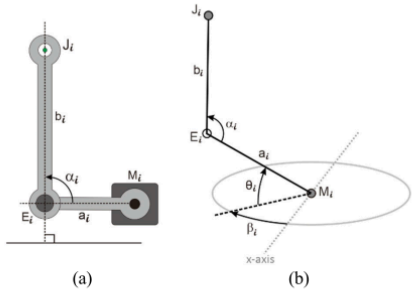

FIGURE 8. The configuration of arm manipulator: (a) arm structure design, (b) system mechanism.

$$J_i x = (a_i . \cos\theta_i + b_i . \cos(\theta_i + \alpha_i)) \cos\beta_i + M_i x \quad (17)$$

$$J_iy = (a_i.\cos\theta_i + b_i.\cos(\theta_i + \alpha_i))\sin\beta_i + M_iy \quad (18)$$

$$J_iz = a_i.\sin\theta_i + b_i.\sin(\theta_i + \alpha_i) + M_iz \quad (19)$$

By applying trigonometric theorems, we obtain,

$$J_ix = (a_i.\cos\theta_i + b_i(\cos\theta_i.\cos\alpha_i - \sin\theta_i.\sin\alpha_i))\cos\beta_i + M_ix \quad (20)$$

$$J_iy = (a_i.\cos\theta_i + b_i(\cos\theta_i.\cos\alpha_i - \sin\theta_i.\sin\alpha_i))\sin\beta_i + M_iy \quad (21)$$

$$J_iz = (a_i.\sin\theta_i + b_i(\sin\theta_i.\cos\alpha_i + \cos\theta_i.\sin\alpha_i)) + M_iz \quad (22)$$

In this condition, the arm b_i remains perpendicular at 90° to the base, even when motor M_i moves. This is because point J_i is connected to the triangular plane above it, keeping arm b_i perpendicular. The simulation of this movement is shown in Figure 9. Based on this condition, the angle $\alpha_i = 90 + \theta_i$, so by applying the rules $\cos(90 + \theta_1) = -\sin\theta_i$ and $\sin(90 + \theta_1) = \cos\theta_i$, we obtain $sin\ \alpha_i = cos\ \theta_i$ and $cos\ \alpha_i = -sin\ \theta_i$. Then, by substituting in Eq. (20), Eq. (21), and Eq. (22), the following equations is derived.

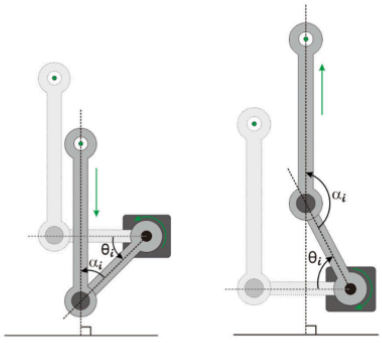

FIGURE 9. Principle work of manipulator arm movement: (a) downward movement, (b) upward movement.

For the point x,

$$J_ix = (a_i.\cos\theta_i + b_i(-\cos\theta_i.\sin\theta_i - \sin\theta_i.\cos\theta_i)\cos\beta_i + M_ix \quad (23)$$

$$J_ix = (a_i.\cos\theta_i + b_i(-2\sin\theta_i.\cos\theta_i)\cos\beta_i + M_ix \quad (24)$$

$$J_ix = (a_i.\cos\theta_i + b_i.\sin 2\theta_i).\cos\beta_i + M_ix \quad (25)$$

For the point y,

$$J_iy = (a_i.\cos\theta_i + b_i(-\cos\theta_i.\sin\theta_i - \sin\theta_i.\cos\theta_i)\sin\beta_i + M_iy \quad (26)$$

$$J_iy = (a_i.\cos\theta_i + b_i(-2\sin\theta_i.\cos\theta_i)\sin\beta_i + M_iy \quad (27)$$

$$J_iy = (a_i.\cos\theta_i + b_i.\sin 2\theta_i).\sin\beta_i + M_iy \quad (28)$$

For the point z,

$$J_iz = (a_i.\sin\theta_i + b_i(-\sin\theta_i.\sin\theta_i + \cos\theta_i.\cos\theta_i) + M_iz \quad (29)$$

$$J_iz = (a_i.\sin\theta_i + b_i\left(1 - 2\sin^2\theta_i\right) + M_iz \quad (30)$$

$$J_iz = a_i.\sin\theta_i + b_i.\cos 2\theta_i + M_iz \quad (31)$$

In the proposed system, the angle β_i varies for each motor. In Figure 10(a), the top view shows the orientation of motors M_1, M_2, and M_3, each connected to arms a_1, a_2, and a_3 at points E_1, E_2, and E_3. The angle between each motor is depicted, with 315° for M_1, 45° for M_2, and 180° for M_3. Meanwhile, Figure 10(b) shows the physical layout or placement positions of the motors and the manipulator arms connected at the same points. These motors are strategically positioned to move each arm accurately.

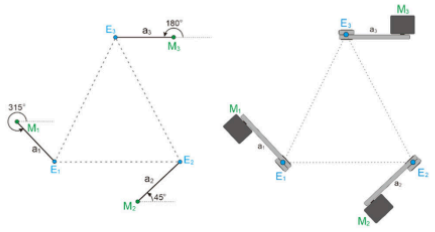

FIGURE 10. The arrangement of servo motors from a top view: (a) orientation of each motor, (b) position of each motor.

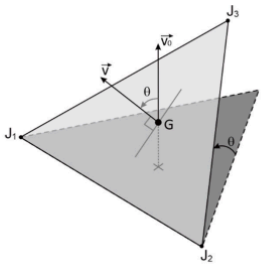

FIGURE 11. The normal vector on the triangular plane.

Next, the tracker system's azimuth and altitude direction are calculated based on each motor's movement angle. To determine these values, it is necessary to calculate the normal vector of the triangular plane, as shown in Figure 11, where $\vec{v_0}$ is the initial normal vector when its direction is perpendicular upward, and $\vec{v}$ is the normal vector when its direction changes. Based on the coordinate points

$J_1\,(x_1, y_1, z_1)$, $J_2\,(x_2, y_2, z_2)$, and $J_3\,(x_3, y_3, z_3)$, the normal vector is calculated using the following equation,

$$\vec{v} = \overrightarrow{J_1J_2} \,.\, \overrightarrow{J_1J_3} \tag{32}$$

where, $\overrightarrow{J_1J_2}$ is the vector from point J_1 to point J_2 and $\overrightarrow{J_1J_3}$ is the vector from point J_1 to point J_3. The vectors in Eq. (32) can be calculated using the following equations,

$$\overrightarrow{J_1J_2} = (x_2 - x_1, y_2 - y_1, z_2 - z_1\,) \tag{33}$$

$$\overrightarrow{J_1J_3} = (x_3 - x_1, y_3 - y_1, z_3 - z_1\,) \tag{34}$$

Thus, from Eq. (33) and Eq. (34), the normal vector is expressed as follows,

$$\vec{v} = \begin{vmatrix} \hat{i} & \hat{j} & \hat{k} \\ x_2 - x_1 & y_2 - y_1 & z_2 - z_1 \\ x_3 - x_1 & y_3 - y_1 & z_3 - z_1 \end{vmatrix} \tag{35}$$

So that, we obtain,

$$v_x = (y_2 - y_1)\,(z_3 - z_1) - (y_3 - y_1)\,(z_2 - z_1) \tag{36}$$

$$v_y = (x_2 - x_1)\,(z_3 - z_1) - (x_3 - x_1)\,(z_2 - z_1) \tag{37}$$

$$v_z = (x_2 - x_1)\,(y_3 - y_1) - (x_3 - x_1)\,(y_2 - y_1) \tag{38}$$

Based on Eq. (36), Eq. (37), and Eq. (38), the tilt angle of the plane concerning the x-axis (θ_x) and the y-axis (θ_y) can be determined using the following equations,

$$\theta_x = \cos^{-1}\left(\frac{v_x}{\sqrt{v_x^2 + v_y^2 + v_z^2}}\right) \tag{39}$$

$$\theta_y = \cos^{-1}\left(\frac{v_y}{\sqrt{v_x^2 + v_y^2 + v_z^2}}\right) \tag{40}$$

Meanwhile, to calculate the tracker azimuth (ϕ_T) and tracker altitude (φ_T), the following equations are used,

$$\phi_T = \tan^{-1}\left(\frac{v_y}{v_x}\right) \tag{41}$$

$$\varphi_T = \tan^{-1}\left(\frac{v_z}{\sqrt{v_x^2 + v_y^2}}\right) \tag{42}$$

Meanwhile, point G is the centroid of the triangle and can be calculated using the following equation,

$$\begin{bmatrix} G_x \\ G_y \\ G_z \end{bmatrix} = \begin{bmatrix} (x_1 + x_2 + x_3)\,/3 \\ (y_1 + y_2 + y_3)\,/3 \\ (z_1 + z_2 + z_3)\,/3 \end{bmatrix} \tag{43}$$

IV. PERFORMANCE ANALYSIS

The analysis provides performance results of each model in predicting PV output power based on its operational temperature. The analytical methods used include calculating Mean Absolute Error (MAE), Root Mean Squared Error (RMSE), Mean Absolute Percentage Error (MAPE), Coefficient of Determination (R^2), and Coefficient of Variation (CV).

MAE is one of the commonly used methods to analyze model performance. It measures the average absolute difference between the predicted values generated by the model and the actual values in the test data. This result shows how closely the model predictions match the actual values overall. The equation for MAE is as follows,

$$MAE = \frac{1}{n}\sum_{i=n}^{n} |y_i - \hat{y}_i| \tag{44}$$

where, n is the number of test data points, y_i is the actual value, and $\hat{y}_i$ is the value predicted by the model for the i data point. A lower MAE value indicates better model performance, signifying that the model's predictions are closer to the actual values [66]. Next, RMSE analysis is conducted by calculating the square root of the average of the squared differences between the model's predicted values and the actual values. The equation for RMSE is defined as follows,

$$RMSE = \sqrt{\frac{1}{n}\sum_{i=n}^{n} (y_i - \hat{y}_i)^2} \tag{45}$$

RMSE analysis indicates the average deviation between the model's predicted and actual values. By taking the square root, RMSE offers a more intuitive interpretation in the same units as the target variable. A lower RMSE value indicates better model performance, meaning the model's predictions are closer to the actual values [67]. Next, MAPE analysis is a method to measure the error rate of a model by calculating the average of the absolute percentage error between the predicted and actual values. The equation for calculating MAPE is defined as follows,

$$MAPE = \frac{1}{n}\sum_{i=n}^{n} \left|\frac{y_i - \hat{y}_i}{y_i}\right| .100\% \tag{46}$$

The MAPE value indicates the prediction error in percentage terms. The lower the MAPE value, the better the model's performance in predicting the data. One advantage of MAPE is its ease of interpretation, as the result is a percentage. Next, the R^2 analysis, known as the Coefficient of Determination, is used to measure how well the developed model can explain the variability in the data. The equation for the Coefficient of Determination is defined as follows,

$$R^2 = 1 - \frac{\sum_{i=1}^{n} (y_i - \hat{y}_i)^2}{\sum_{i=1}^{n} (y_i - \hat{y})^2} \tag{47}$$

where, $\hat{y}$ is the mean of all y_i values. The R^2 value ranges from 0 to 1, where a value closer to 1 indicates that the model better explains the variability in the data. R^2 analysis can determine how much output data variability can be explained by the input data. Lastly, the CV analysis, or Coefficient of Variation, is a statistical measure to assess a dataset's relative degree of variation. CV is defined as the ratio of the standard

deviation to the mean, expressed as follows,

$$CV = \frac{\sqrt{\frac{1}{n}\sum_{i=1}^{n}\left(y_i - \frac{1}{n}\sum_{i=1}^{n} y_i\right)^2}}{\frac{1}{n}\sum_{i=1}^{n} y_i} \quad (48)$$

CV is typically used to measure data stability. A low CV value indicates more stable data, while a high CV value suggests more significant variability in the data.

V. RESULTS AND DISCUSSION

In this section, an evaluation is conducted to assess the performance of ANFIS in each model based on the type of consequent rule. Then, the movement of the three motors is simulated to obtain the azimuth and altitude angles. Testing uses the sun tracker device to assess the system's ability to track the sun's position. Finally, comparing previous systems is necessary to validate the proposed sun tracker system's effectiveness.

A. MODEL PERFORMANCE ANALYSIS

Table 4 presents the statistical results from the model's training and testing phases based on three types of consequent rules: first-order, second-order, and third-order. The dataset consists of 80% for training and 20% for testing. The ANFIS training and testing results show that the choice of consequent rule significantly impacts each model's performance.

In ANFIS model 1, the second-order performed best compared to the first-order and third-order, both in the training and testing phases. During training, the second-order achieved the lowest MAE, RMSE, and MAPE values, at 3.6, 4.5, and 8.08%, respectively, along with a high R^2 value of 0.98. This result indicates that the model can predict motor movement accurately based on the input data. In testing, the second-order also excelled with the lowest MAE, RMSE, and MAPE values, at 2.82, 3.34, and 7.02%, respectively, indicating accurate model performance with minimal error. In ANFIS model 2, a similar pattern emerged, with the second-order demonstrating optimal performance. During training, the second-order model yielded low MAE, RMSE, and MAPE values of 3.82, 4.74, and 8.3%, along with a high R^2 value of 0.97. In testing, the second-order produced MAE, RMSE, and MAPE values of 3, 3.58, and 6.44%, respectively, outperforming the first-order and third-order models. In ANFIS model 3, the second-order also provided the best results, achieving the lowest error values in training with MAE, RMSE, and MAPE of 3.8, 4.68, and 7.69%, respectively, and the highest R^2 value of 0.98. However, in testing, the second-order's performance was less optimal than the third-order, as indicated by higher MAE, RMSE, and MAPE values than the third-order. The training and testing analysis results show that the second-order consequent rule is optimal for all three ANFIS models.

Figure 12(a) displays the motor movement results with different consequent rules. The graph shows that all three consequent rules follow the angle change patterns quite well, although first-order shows more significant discrepancies.

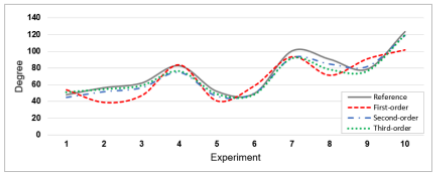

(a)

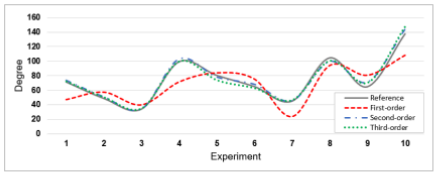

(b)

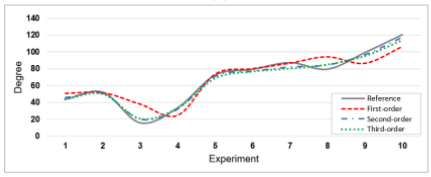

(c)

FIGURE 12. The comparison analysis of consequence rule variations to controlling motor movements (a) ANFIS 1 model, (b) ANFIS 2 model, (c) ANFIS 3 model.

Meanwhile, in Figure 12(b), the first-order consequent rule exhibits noticeable differences, especially in the sixth and eighth experiments. On the other hand, second-order and third-order are more consistent in approaching the actual angle, although slight differences still exist at some points. In Figure 12(c), the average difference between the actual angle and the angle produced by each consequent rule is more minor than the previous graph. Overall, although both second-order and third-order consequent rules accurately follow the angle change patterns of all three motors, there are some points where the second-order performs better than the third-order. Figure 13 shows a three-dimensional graph illustrating the relationship between the ratio of two phototransistor values and the output as the motor angle increments for each consequent rule. The comparison values from the two phototransistor readings directly affect the magnitude of the resulting angle increment. In the first-order consequent, the angle increment pattern appears linear. In the second-order consequent, a significant angle increment occurs with more considerable phototransistor ratio differences; the greater the difference, the higher the angle increment. Conversely, there is no considerable angle increase for ratios closer in value. In the third-order, the angle increment pattern is similar to the second-order but displays fluctuations or a nonlinear pattern

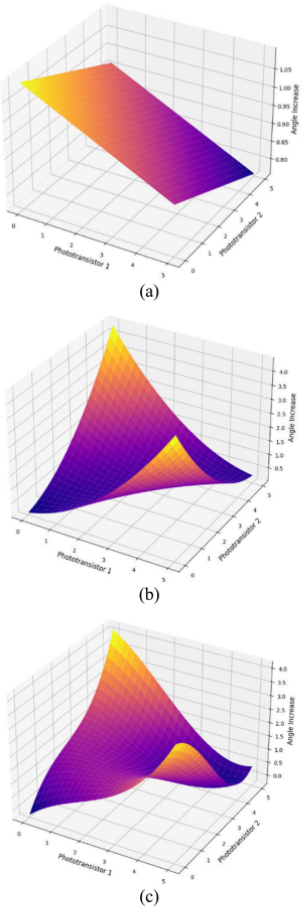

FIGURE 13. The relationship between the phototransistor ratio values with the motor angle increases based on various consequent rules: (a) first-order, (b) second-order, and (c) third-order.

in the middle of the graph. This indicates that there are points where small changes in the phototransistor ratio can lead to a lower or even decreasing angle increment.

After obtaining the model, a motor movement simulation was conducted on the sun tracker to observe the relationship between the movements of the three motors and changes in azimuth and altitude angles. Figure 14 displays the simulation results, showing how each motor's activity influences the panel's orientation changes. In this simulation, it demonstrates the condition where the three motors move at angles

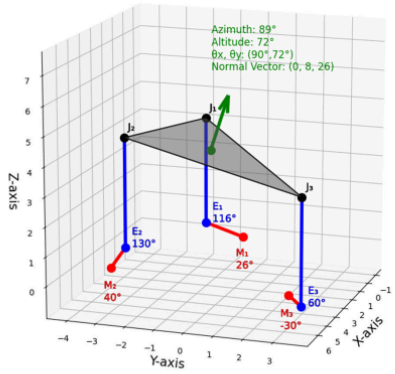

FIGURE 14. The simulation of azimuth and altitude changes based on motor movement ($M_1 = 26°$, $M_2 = 40°$, $M_3 = -30°$).

$M_1 = 26°$, $M_1 = 40°$, and $M_1 = -30°$, resulting in a normal vector direction of (0, 8, 26) with tilt angles of $\theta_x = 90°$ and $\theta_y = 72°$. Meanwhile, the resulting azimuth and altitude angles are 89° and 72°, respectively. Further testing results are shown in Figure 15, combining an angle range of $-30°$ to 90°, representing the minimum to maximum motor angles. Figure 15(a) shows that the azimuth angle ranges from 0° to 360°, while Figure 15(b) indicates that the altitude angle ranges from 60° to 90°. This angle range demonstrates that the triple-axis mechanism can achieve good orientation flexibility, allowing the system to adjust the PV panel position effectively to minimize the solar incidence angle.

Subsequent testing was conducted to analyze the response of the sun tracker system in mitigating uncertain disturbances, such as the continuous movement of light due to cloud movement or shadows from external objects. The testing scenario involved observing the movement of the sun tracker at azimuth and altitude angles of 89° and 72°, respectively. The results of the sun tracker system's response based on ANFIS consequent rules are shown in Figure 16. Based on these tests, the proposed control rules were able to mitigate the effects of disturbances, such as changes in light intensity due to clouds, while maintaining the optimal orientation of the solar panel. Under partial shading conditions, where some sensors or PV panels receive reduced light intensity due to shadows from clouds or surrounding objects, the tracking system may face challenges in maintaining the optimal orientation of the solar panel toward the sun.

Further analysis was conducted to determine the system's response to each ANFIS consequent rule in response to changes in light position. The study was performed by comparing the system's response based on Figure 16. This analysis considered characteristics such as rise time, peak time, overshoot, settling time, and steady-state error for both

TABLE 4. The results of ANFIS training and testing with various consequent rules.

Model	Parameter	Training			Testing		
		First-Order	Second-Order	Third-Order	First-Order	Second-Order	Third-Order
ANFIS 1	MAE	9.3	3.6	5.26	9.57	2.82	4.08
	RMSE	11.61	4.5	6.21	11.33	3.34	4.95
	MAPE	21.79%	8.08%	17.08%	21.78%	7.02%	10.5%
	R^2	0.81	0.98	0.96	0.83	0.99	0.97
	CV	0.39	0.49	0.47	0.42	0.47	0.44
ANFIS 2	MAE	11.09	3.82	5.08	9.79	3	3.51
	RMSE	13.78	4.74	6.05	11.81	3.58	4.33
	MAPE	19.44%	8.3%	12.86%	21.57%	6.44%	8.79%
	R^2	0.69	0.97	0.95	0.82	0.99	0.98
	CV	0.3	0.42	0.4	0.4	0.46	0.46
ANFIS 3	MAE	11.76	3.8	4.41	8.94	2.86	2.77
	RMSE	14.1	4.68	5.33	10.86	3.48	3.4
	MAPE	22.83%	7.69%	8.83%	18.52%	6.35%	6.11%
	R^2	0.7	0.98	0.97	0.85	0.99	0.99
	CV	0.35	0.48	0.43	0.41	0.47	0.47

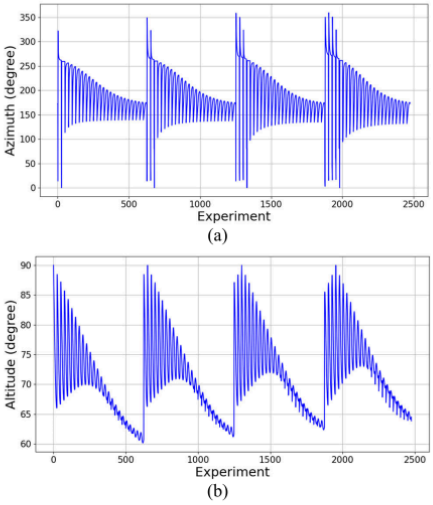

FIGURE 15. The results of the sun tracker movement experiment based on all combinations of angles M_1, M_2, and M_3: (a) azimuth angle movement and (b) altitude angle movement.

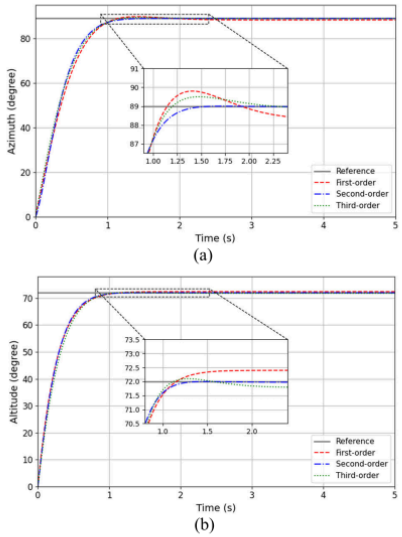

FIGURE 16. The comparison result of responses to light changes for each ANFISconsequent rules (a) azimuth movement, (b) altitude movement.

azimuth and altitude movements, which are presented in Table 5 and Table 6. For azimuth movement, second-order showed the most optimal performance, achieving the fastest rise time and settling time with low steady-state error. The second-order response also did not exhibit any overshoot. Meanwhile, the peak time obtained was longer than that of the

first-order. In the first-order, the settling time was unavailable because the system response did not reach a steady-state condition during the observation period. For altitude movement, the analysis also indicated that the second-order performed better than the others. No overshoot occurred in the second-order, as with the azimuth movement. In the first-order, the settling time was also unavailable, as the system response did not reach a steady-state condition. This analysis reveals that second-order is the best choice for controlling both azimuth and altitude movements, making this consequent rule most suitable for implementation in ANFIS-PCT for a triple-axis sun tracker system.

TABLE 5. The comparison of performance ANFIS consequent rules on azimuth movement.

Parameter	First-order	Second-order	Third-order
Rise Time (s)	0.681	0.601	0.661
Peak Time (s)	1.403	1.723	1.483
Overshoot (%)	0.899	0	0.562
Settling Time (s)	-	1.462	2.212
Steady State Error	0.679	0.03	0.111

TABLE 6. The comparison of performance ANFIS consequent rules on altitude movement.

Parameter	First-order	Second-order	Third-order
Rise Time (s)	0.511	0.491	0.521
Peak Time (s)	2.685	1.493	1.283
Overshoot (%)	0.556	0	0.139
Settling Time (s)	-	1.34	1.538
Steady State Error	0.399	0.027	0.213

B. SUN TRACKER SYSTEM PERFORMANCE ANALYSIS

Figure 17(a) compares the sun tracker movement and the azimuth angle of the actual sun position. The graph shows the sun tracker accurately follows the sun's azimuth angle from sunrise to sunset. Meanwhile, Figure 17(b) compares the altitude angle. Based on this graph, a discrepancy occurs at the start of tracking, around 7:00 AM to 8:00 AM. Then, the sun tracker successfully tracks the sun's altitude more accurately, reaching a peak at 12:30 PM at its maximum altitude. Afterwards, the altitude of the sun tracker gradually decreases in sync with the sun's position until sunset. Overall, the sun tracker system works effectively to adjust its movement in tracking the sun's position in azimuth and altitude angles, thereby minimizing the solar incidence angle on the PV surface throughout the day.

C. SYSTEM PERFORMANCE COMPARISON

Table 7 compares the proposed ANFIS model's performance with several previous models related to sun tracker systems. The comparison aims to validate the performance of the proposed ANFIS model in tracking the sun's position. The models compared include PID-ANN [44], Fast Integral Terminal Sliding Mode Control (FIT-SMC) [68], Neural Network Algorithm with Model Predictive Control (NNA-MPC) [69], PID with Internal Model Controller (PID-IMC) [51], PID with Fuzzy Logic Controller (PID-FLC) [48], PD with Fuzzy Logic Controller (PD-FLC) [46], and Artificial Bee Colony (ABC) [50]. The parameters compared are rise time, settling time, and steady-state error. Based on the comparison, the proposed ANFIS-PCT model demonstrates optimal performance. For the rise time parameter, ANFIS-PCT has a relatively fast time, only behind the FIT-SMC model, which recorded the most rapid rise time of 0.15 seconds. However, compared to other models, ANFIS-PCT is far superior. For the settling time parameter, ANFIS-PCT also shows optimal performance, although it is still behind FIT-SMC, which recorded the fastest time. Meanwhile, for the steady-state error, ANFIS-PCT demonstrates a more stable and accurate system.

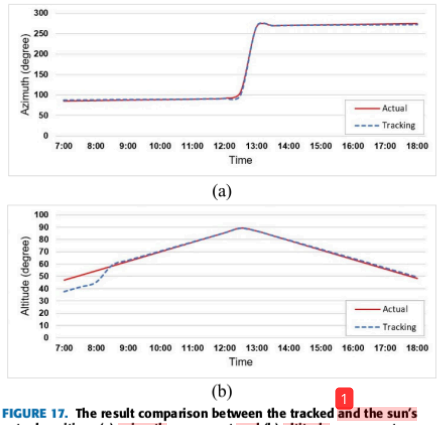

FIGURE 17. The result comparison between the tracked and the sun's actual position: (a) azimuth movement and (b) altitude movement.

TABLE 7. The comparison of the proposed ANFIS model with other published models.

Model	Rise Time (s)	Settling Time (s)	Steady State Error
ANFIS-PCT (Proposed)	0.55	1.4	0.03
PID-ANN	2.18	2.46	0.07
FIT-SMC	0.15	0.33	-
NNA-MPC	-	0.108	-
PID-IMC	1.8	5.58	-
PID-FLC	3.6	4.8	0.4
PD-FLC	6.38	6.38	0.83
ABC	2.37	5.23	1.05

VI. CONCLUSION

Based on the analysis results, all three proposed ANFIS models using the second-order consequent rule deliver the

best performance compared to the first-order and third-order, both in the training and testing phases. The simulation results show that the movement of the sun tracker with a triple-axis mechanism can reach an azimuth angle ranging from 0° to 360°. In contrast, the altitude angle ranges from 60° to 90°. These values indicate that the sun tracker has good flexibility. The proposed system has nonlinear dynamics, so several parameters must be continuously optimized through the training process to gradually reduce the error value in the system until it approaches zero. This indicates that the system will always move towards stability, even with small variations in input parameters or disturbances.

Although the proposed sun tracker system offers improved accuracy and responsiveness in tracking the sun's position, it has some drawbacks, including system complexity, leading to higher energy consumption. This is due to the number of motors that need to move simultaneously to reach the optimal position. The additional energy the motors consume in the triple-axis mechanism can reduce overall energy efficiency, especially in conditions with limited energy sources.

Future research will focus on developing triple-axis sun tracker technology techniques to enhance efficiency by reducing energy consumption and optimizing PCT in ANFIS to make it more adaptive in tracking the sun's position. Further research can be developed by exploring the Lyapunov method to explicitly determine the stability of the sun tracker system, allowing the mathematical proof to support the experimental results that have been conducted. Additionally, future research will focus on exploring energy-saving strategies, including optimizing by reducing unnecessary servo motor movements, as well as evaluating the comparison between the energy produced and the total energy consumed.

REFERENCES

[1] L. Salgado-Conrado, "A review on sun position sensors used in solar applications," *Renew. Sustain. Energy Rev.*, vol. 82, pp. 2128–2146, Feb. 2018, doi: 10.1016/j.rser.2017.08.040.

[2] A. Alshaabani, "Developing the design of single-axis sun sensor solar tracking system," *Energies*, vol. 17, no. 14, p. 3442, Jul. 2024, doi: 10.3390/en17143442.

[3] H. D. Kambezidis, K. Mimidis, and K. A. Kavadias, "The solar energy potential of Greece for flat-plate solar panels mounted on double-axis systems," *Energies*, vol. 16, no. 13, p. 5067, Jun. 2023, doi: 10.3390/en16135067.

[4] Y. Away, Syahrizal, H. Walidainy, M. S. Rizal, and A. Novandri, "Artificial neural network technique to predict the sun position in cloudy state with tetrahedron based sensor," in *Proc. Int. Conf. Comput. Syst., Inf. Technol., Electr. Eng. (COSITE)*, Oct. 2021, pp. 134–137, doi: 10.1109/COSITE52651.2021.9649550.

[5] Y. Away, A. Rahman, T. R. Auliandra, and M. Firdaus, "Performance comparison between PID and fuzzy algorithm for sun tracker based on tetrahedron geometry sensor," in *Proc. Int. Conf. Electr. Eng. Informat. (ICELTICs)*, Sep. 2018, pp. 40–44, doi: 10.1109/ICELTICS.2018.8548837.

[6] K. B. D. Melo, H. S. Moreira, and M. G. Villalva, "Influence of solar position calculation methods applied to horizontal single-axis solar trackers on energy generation," *Energies*, vol. 13, no. 15, p. 3826, Jul. 2020, doi: 10.3390/en13153826.

[7] S. I. Palomino-Resendiz, F. A. Ortiz-Martínez, I. V. Paramo-Ortega, J. M. González-Lira, and D. A. Flores-Hernández, "Optimal selection of the control strategy for dual-axis solar tracking systems," *IEEE Access*, vol. 11, pp. 56561–56573, 2023, doi: 10.1109/ACCESS.2023.3283336.

[8] N. C. Alparslan, A. Kayabasi, and S. E. Rusen, "Estimation of global solar radiation by using ANN and ANFIS," in *Proc. Innov. Intell. Syst. Appl. Conf. (ASYU)*, Oct. 2019, pp. 1–6, doi: 10.1109/ASYU48272.2019.8946448.

[9] Y. Away, A. Novandri, and M. S. Rizal, "Analysis of energy harvesting on 3-DOF mobile tetrahedron-based sun tracker," *IOP Conf. Series, Earth Environ. Sci.*, vol. 1356, no. 1, Jun. 2024, Art. no. 012087, doi: 10.1088/1755-1315/1356/1/012087.

[10] D. A. Flores-Hernández, A. Luviano-Juárez, N. Lozada-Castillo, O. Gutiérrez-Frías, C. Domínguez, and I. Antón, "Optimal strategy for the improvement of the overall performance of dual-axis solar tracking systems," *Energies*, vol. 14, no. 22, p. 7795, Nov. 2021, doi: 10.3390/en14227795.

[11] N. G. Hariri, M. A. AlMutawa, I. S. Osman, I. K. AlMadani, A. M. Almahdi, and S. Ali, "Experimental investigation of Azimuth- and sensor-based control strategies for a PV solar tracking application," *Appl. Sci.*, vol. 12, no. 9, p. 4758, May 2022, doi: 10.3390/app12094758.

[12] C. R. J. Doss, M. Kumaravel, and V. J. Kumar, "A novel measurement technique for performance comparison of sun tracker systems," in *Proc. IEEE Int. Instrum. Meas. Technol. Conf. (I2MTC)*, May 2013, pp. 1156–1160, doi: 10.1109/I2MTC.2013.6555595.

[13] M. Engin, "Controller design for parallel mechanism solar tracker," *Machines*, vol. 11, no. 3, p. 372, Mar. 2023, doi: 10.3390/machines11030372.

[14] M. H. M. Sidek, N. Azis, W. Z. W. Hasan, M. Z. A. A. Kadir, S. Shafie, and M. A. M. Radzi, "Automated positioning dual-axis solar tracking system with precision elevation and azimuth angle control," *Energy*, vol. 124, pp. 160–170, Apr. 2017, doi: 10.1016/j.energy.2017.02.001.

[15] A. Musa, E. Alozie, S. A. Suleiman, J. A. Ojo, and A. L. Imoize, "A review of time-based solar photovoltaic tracking systems," *Information*, vol. 14, no. 4, p. 211, Mar. 2023, doi: 10.3390/info14040211.

[16] K. Kumar, L. Varshney, A. Ambikapathy, V. Mittal, S. Prakash, P. Chandra, and N. Khan, "Soft computing and IoT based solar tracker," *Int. J. Power Electron. Drive Syst. (IJPEDS)*, vol. 12, no. 3, p. 1880, Sep. 2021, doi: 10.11591/ijpeds.v12.i3.pp1880-1889.

[17] S. Aziz and M. Hassan, "Dual axis solar tracker for solar panel with wireless switching," in *Proc. Int. Conf. Microelectron., Comput. Commun. Syst. (MCCS)*, 2019, pp. 49–62, doi: 10.1007/978-981-10-8234-4_6.

[18] Y. Away, Y. Yanti, M. S. Rizal, and A. Novandri, "Interactive control using Bluetooth for dual axis sun tracker with three light sensors," in *Proc. Int. Conf. Educ., Sci. Technol.*, 2019, pp. 1–9, doi: 10.1088/1742-6596/1232/1/012038.

[19] H. Fathabadi, "Novel online sensorless dual-axis sun tracker," *IEEE/ASME Trans. Mechatronics*, vol. 22, no. 1, pp. 321–328, Feb. 2017, doi: 10.1109/TMECH.2016.2611564.

[20] H. Fathabadi, "Comparative study between two novel sensorless and sensor based dual-axis solar trackers," *Sol. Energy*, vol. 138, pp. 67–76, Nov. 2016, doi: 10.1016/j.solener.2016.09.009.

[21] Y. Away and M. Ikhsan, "Dual-axis sun tracker sensor based on tetrahedron geometry," *Autom. Construction*, vol. 73, pp. 175–183, Jan. 2017, doi: 10.1016/j.autcon.2016.10.009.

[22] H. A. Lastya, Y. Away, I. D. Sara, M. Ikhsan, and N. M. Mirdha, "Development of dual-axis sun tracker based on tetrahedron geometry using phototransistor sensor," in *Proc. Comput. Electr. Educ. Res. (PROCESSOR)*, 2023, pp. 91–102.

[23] H. A. Lastya, Y. Away, T. Tarmizi, I. D. Sara, and M. Ikhsan, "Effect difference size of tetrahedron sun tracker based on sensor for energy harvesting," in *Proc. Int. Conf. Comput. Sci., Inf. Technol. Eng. (ICCoSITE)*, Feb. 2023, pp. 111–116, doi: 10.1109/ICCOSITE57641.2023.10127761.

[24] M. R. Haider, A. Shufian, Md. N. Alam, M. I. Hossain, R. Islam, and Md. A. Azim, "Design and implementation of three-axis solar tracking system with high efficiency," in *Proc. Int. Conf. Inf. Commun. Technol. Sustain. Develop. (ICICT4SD)*, Feb. 2021, pp. 1–5, doi: 10.1109/ICICT4SD50815.2021.9396779.

[25] P. Gupta, V. Gupta, M. Sharma, R. K. Pachauri, and J. Akhtar, "Design and performance analysis of three axis solar tracking system," in *Proc. 7th Asia Conf. Power Electr. Eng. (ACPEE)*, Apr. 2022, pp. 1876–1880, doi: 10.1109/ACPEE53904.2022.9783762.

[26] A. A. A. E. P. Kesava and W. Lim, "Triple-axis tracking control algorithm for maximizing solar energy harvesting on a moving platform," *ARPN J. Eng. Appl. Sci.*, vol. 13, no. 16, pp. 4617–4624, 2018.

[27] C. S. Esobinenwu, "Optimization of solar PV system using anfis controller under partially shaded condition," *Adv. J. Sci. Eng. Technol.*, vol. 8, no. 3, pp. 1–8, 2023.

[28] A. Al-Hmouz, J. Shen, R. Al-Hmouz, and J. Yan, "Modeling and simulation of an adaptive neuro-fuzzy inference system (ANFIS) for mobile learning," *IEEE Trans. Learn. Technol.*, vol. 5, no. 3, pp. 226–237, Jul. 2012, doi: 10.1109/TLT.2011.36.

[29] N. Khan, D. A. Elizondo, L. Deka, and M. A. Molina-Cabello, "Fuzzy logic applied to system monitors," *IEEE Access*, vol. 9, pp. 56523–56538, 2021, doi: 10.1109/ACCESS.2021.3072239.

[30] M. M. Madebo, "Neuro-Fuzzy-Based adaptive sliding mode control of quadrotor UAV in the presence of matched and unmatched uncertainties," *IEEE Access*, vol. 12, pp. 117745–117760, 2024, doi: 10.1109/ACCESS.2024.3447474.

[31] C.-F. Juang and C.-D. Hsieh, "A fuzzy system constructed by rule generation and iterative linear SVR for antecedent and consequent parameter optimization," *IEEE Trans. Fuzzy Syst.*, vol. 20, no. 2, pp. 372–384, Apr. 2012, doi: 10.1109/TFUZZ.2011.2174997.

[32] C. Imron, I. Abadi, I. A. Akbar, J. Maknunah, Y. A. Nor, and A. S. Uyun, "Performance comparison of the single axis and two-axis solar system using adaptive neuro-fuzzy inference system controls," *E3S Web Conf.*, vol. 190, pp. 1–11, Sep. 2020, doi: 10.1051/e3sconf/202019000005.

[33] N. Hadroug, A. Hafaifa, A. Iratni, and M. Guemana, "Reliability modeling using an adaptive neuro-fuzzy inference system: Gas turbine application," *Fuzzy Inf. Eng.*, vol. 13, no. 2, pp. 154–183, Apr. 2021, doi: 10.1080/16168658.2021.1915451.

[34] H. Chaudhary, V. Panwar, N. Sukavanam, and B. Chahar, "Imperialist competitive algorithm optimised adaptive neuro fuzzy controller for hybrid force position control of an industrial robot manipulator: A comparative study," *Fuzzy Inf. Eng.*, vol. 12, no. 4, pp. 435–451, Oct. 2020, doi: 10.1080/16168658.2021.1921378.

[35] M. E. Shalabi, A. M. R. Fath Elbab, H. El-Hussieny, and A. A. Abouelsoud, "Neuro-fuzzy volume control for quarter car air-spring suspension system," *IEEE Access*, vol. 9, pp. 77611–77623, 2021, doi: 10.1109/ACCESS.2021.3081872.

[36] M. Ali, H. Nurohmah, Budiman, J. Suharsono, H. Suyono, and M. A. Muslim, "Optimization on PID and ANFIS controller on dual axis tracking for photovoltaic based on firefly algorithm," in *Proc. Int. Conf. Electr., Electron. Inf. Eng. (ICEEIE)*, vol. 6, Oct. 2019, pp. 1–5, doi: 10.1109/ICEEIE47180.2019.8981428.

[37] N. Al-Rousan, N. A. M. Isa, and M. K. M. Desa, "Efficient single and dual axis solar tracking system controllers based on adaptive neural fuzzy inference system," *J. King Saud Univ.-Eng. Sci.*, vol. 32, no. 7, pp. 459–469, Nov. 2020, doi: 10.1016/j.jksues.2020.04.004.

[38] S. Z. M. Noor, "The analysis of dual axis solar tracking system controllers based on adaptive neural fuzzy inference system (ANFIS)," *J. Mech. Eng.*, vol. 20, no. 2, pp. 167–184, Apr. 2023, doi: 10.24191/jmeche.v20i2.22061.

[39] H. Abouobaida, Y. Mchaouar, S. Ullah, Y. Abouelmahjoub, H. Alghamdi, B. Alghamdi, and H. Kraiem, "Integrated control design for hybrid grid-photovoltaic systems in distillation applications: A reference model and fuzzy logic approach," *Sustainability*, vol. 16, no. 17, p. 7304, Aug. 2024, doi: 10.3390/su16177304.

[40] M. Schwenzer, M. Ay, T. Bergs, and D. Abel, "Review on model predictive control: An engineering perspective," *Int. J. Adv. Manuf. Technol.*, vol. 117, nos. 5–6, pp. 1327–1349, Nov. 2021, doi: 10.1007/s00170-021-07682-3.

[41] H. Matsui, "Quadratic regression for functional response models," *Econometrics Statist.*, vol. 13, pp. 125–136, Jan. 2020, doi: 10.1016/j.ecosta.2018.12.003.

[42] A. Habibi, B. Yousefi, A. N. Shirazi, and M. Rezvani, "Adaptive neuro-fuzzy damping controller of grid-connected microgrid hybrid system integrating wind farms and batteries," *IEEE Access*, vol. 12, pp. 8022–8037, 2024, doi: 10.1109/ACCESS.2023.3312272.

[43] A. Rahman, K. M. Aung, S. Ihsan, R. M. R. A. Shah, M. A. Qubeissi, and M. T. Aljarrah, "Solar energy dependent supercapacitor system with ANFIS controller for auxiliary load of electric vehicles," *Energies*, vol. 16, no. 6, p. 2690, Mar. 2023, doi: 10.3390/en16062690.

[44] Y. Away, A. Novandri, I. Raziah, and M. Melinda, "A new technique for improving the precision of dual-axis tetrahedron-based sensor with switching between PID and ANN," *IEEE Access*, vol. 11, pp. 89138–89151, 2023, doi: 10.1109/ACCESS.2023.3305944.

[45] M. Melinda, A. Novandri, and Y. Away, "PID controllers performance on dual axis tracking with tetrahedron based sensor," *Kinetik, Game Technol., Inf. Syst., Comput. Netw., Comput., Electron., Control*, vol. 7, no. 4, pp. 371–382, Nov. 2022, doi: 10.22219/kinetik.v7i4.1549.

[46] F. Rahmah, F. Hidayanti, E. K. Wati, K. R. Lestari, and S. W. Sudrajat, "Solar panel motor tracker model comparison between PID and fuzzy PD," *Int. J. Renew. Energy Res.*, vol. 12, no. 3, pp. 1427–1434, 2022, doi: 10.20508/ijrer.v12i3.13117.g8525.

[47] B. Baisrum, B. Setiadi, S. Sudrajat, V. Wijayakusuma, H. Ulhaq, R. Hikmawati, N. Qamaruddin, and S. Hardiansyah, "Implementation of adaptive neuro-fuzzy inference system control on pneumatic solar tracker," in *Proc. 2nd Int. Seminar Sci. Appl. Technol. (ISSAT)*, 2021, pp. 422–429, doi: 10.2991/aer.k.211106.067.

[48] I. Abadi, A. Musyafa', W. Z. Putra, and D. N. Fitriyanah, "Performance analysis of dual axis solar tracker based on fuzzy PID controller on street lighting," in *Proc. Int. Conf. Comput. Eng., Netw., Intell. Multimedia (CENIM)*, Nov. 2020, pp. 257–263, doi: 10.1109/CENIM51130.2020.9297938.

[49] J. Faraji, M. Khanjanianpak, M. Rezaei, M. Kia, E. Aliyan, and P. Dehghanian, "Fast-accurate dual-axis solar tracker controlled by P&O technique with neural network optimization," in *Proc. IEEE Int. Conf. Environ. Electr. Eng. IEEE Ind. Commercial Power Syst. Eur. (EEEIC/I CPS Eur.)*, Jun. 2020, pp. 1–6, doi: 10.1109/eeeic/icpseurope49358.2020.9160843.

[50] Z. A. Yusuf, A. T. Salawudeen, and H. Bege. (2019). *Tracking and Control of DC Motor for PV Systems Positioning Using Artificial Bee Colony Algorithm*. [Online]. Available: https://www.academia.edu/download/65461382/solar2018.pdf

[51] B. O. Oladayo and A. O. Titus, "Development of solar tracking system using IMC-PID controller," *Amer. J. Eng. Res.*, vol. 5, no. 5, pp. 135–142, 2016.

[52] M. M. Sabir and T. Ali, "Optimal PID controller design through swarm intelligence algorithms for sun tracking system," *Appl. Math. Comput.*, vol. 274, pp. 690–699, Feb. 2016, doi: 10.1016/j.amc.2015.11.036.

[53] N. Li and S.-Y. Li, "Stability analysis and design of T-S fuzzy control system with simplified linear rule consequent," *IEEE Trans. Syst., Man Cybern., B, Cybernetics*, vol. 34, no. 1, pp. 788–795, Feb. 2004, doi: 10.1109/TSMCB.2003.817060.

[54] L. Yingjie and W. Baoshu, "Study on the control course of ANFIS based aircraft auto-landing," *J. Syst. Eng. Electron.*, vol. 16, no. 3, pp. 583–587, Sep. 2005.

[55] G. V. Lakhekar, L. M. Waghmare, P. G. Jadhav, and R. G. Roy, "Robust diving motion control of an autonomous underwater vehicle using adaptive neuro-fuzzy sliding mode technique," *IEEE Access*, vol. 8, pp. 109891–109904, 2020, doi: 10.1109/ACCESS.2020.3001631.

[56] A. M. M. Al-Qaysi, A. Bozkurt, and Y. Ateş, "Load forecasting based on genetic algorithm–artificial neural network-adaptive neuro-fuzzy inference systems: A case study in Iraq," *Energies*, vol. 16, no. 6, p. 2919, Mar. 2023, doi: 10.3390/en16062919.

[57] P. Cortés-Antonio, I. Batyrshin, A. Martínez-Cruz, L. A. Villa-Vargas, M. A. Ramírez-Salinas, I. Rudas, O. Castillo, and H. Molina-Lozano, "Learning rules for sugeno ANFIS with parametric conjunction operations," *Appl. Soft Comput.*, vol. 89, Apr. 2020, Art. no. 106095, doi: 10.1016/j.asoc.2020.106095.

[58] B. Saleem, R. Badar, A. Manzoor, M. A. Judge, J. Boudjadar, and S. U. Islam, "Fully adaptive recurrent neuro-fuzzy control for power system stability enhancement in multi machine system," *IEEE Access*, vol. 10, pp. 36464–36476, 2022, doi: 10.1109/ACCESS.2022.3164455.

[59] A. F. Bendary, A. Y. Abdelaziz, M. M. Ismail, K. Mahmoud, M. Lehtonen, and M. M. F. Darwish, "Proposed ANFIS based approach for fault tracking, detection, clearing and rearrangement for photovoltaic system," *Sensors*, vol. 21, no. 7, p. 2269, Mar. 2021, doi: 10.3390/s21072269.

[60] A. A. Rizvi, K. Addoweesh, A. El-Leathy, and H. Al-Ansary, "Sun position algorithm for sun tracking applications," in *Proc. 40th Annu. Conf. IEEE Ind. Electron. Soc. (IECON)*, Oct. 2014, pp. 5595–5598, doi: 10.1109/IECON.2014.7049356.

[61] A. Awasthi, A. K. Shukla, S. R. M. Manohar, C. Dondariya, K. N. Shukla, D. Porwal, and G. Richhariya, "Review on sun tracking technology in solar PV system," *Energy Rep.*, vol. 6, pp. 392–405, Nov. 2020, doi: 10.1016/j.egyr.2020.02.004.

[62] V. Radhakrishna, P. V. Kumar, S. A. Aljawarneh, and V. Janaki, "Design and analysis of a novel temporal dissimilarity measure using Gaussian membership function," in *Proc. Int. Conf. Eng. MIS (ICEMIS)*, May 2017, pp. 1–5, doi: 10.1109/ICEMIS.2017.8273098.

[63] J. Botzheim, E. Lughofer, E. P. Klement, L. T. Koczy, and T. T. D. Gedeon, "Separated antecedent and consequent learning for Takagi–Sugeno fuzzy systems," in *Proc. IEEE Int. Conf. Fuzzy Syst.*, Aug. 2006, vol. 1, no. 1, pp. 2263–2269, doi: 10.1109/FUZZY.2006.1682014.

[64] P. J. Parikh and S. S. Y. Lam, "A hybrid strategy to solve the forward kinematics problem in parallel manipulators," *IEEE Trans. Robot.*, vol. 21, no. 1, pp. 18–25, Feb. 2005, doi: 10.1109/TRO.2004.833801.
[65] P. J. Parikh and S. S. Lam, "Solving the forward kinematics problem in parallel manipulators using an iterative artificial neural network strategy," *Int. J. Adv. Manuf. Technol.*, vol. 40, nos. 5–6, pp. 595–606, Jan. 2009, doi: 10.1007/s00170-007-1360-x.
[66] W. Wang and Y. Lu, "Analysis of the mean absolute error (MAE) and the root mean square error (RMSE) in assessing rounding model," *IOP Conf. Ser., Mater. Sci. Eng.*, vol. 324, no. 1, Mar. 2018, Art. no. 012049, doi: 10.1088/1757-899x/324/1/012049.
[67] T. Chai and R. R. Draxler, "Root mean square error (RMSE) or mean absolute error (MAE)?—Arguments against avoiding RMSE in the literature," *Geosci. Model Develop.*, vol. 7, no. 3, pp. 1247–1250, Jun. 2014, doi: 10.5194/gmd-7-1247-2014.
[68] K. Ali, S. Ullah, A. Mehmood, H. Mostafa, M. Marey, and J. Iqbal, "Adaptive FIT-SMC approach for an anthropomorphic manipulator with robust exact differentiator and neural network-based friction compensation," *IEEE Access*, vol. 10, pp. 3378–3389, 2022, doi: 10.1109/ACCESS.2021.3139041.
[69] M. Elsisi, K. Mahmoud, M. Lehtonen, and M. M. F. Darwish, "Effective nonlinear model predictive control scheme tuned by improved NN for robotic manipulators," *IEEE Access*, vol. 9, pp. 64278–64290, 2021, doi: 10.1109/ACCESS.2021.3075581.

HARI ANNA LASTYA (Student Member, IEEE) was born in Banda Aceh, Aceh, in April 1987. She received the degree from the Department of Electrical Engineering, Faculty of Engineering, Universitas Syiah Kuala (USK), Banda Aceh, in 2009, and the master's degree from the Department of Electrical Engineering, Faculty of Engineering, Universitas Sumatera Utara, Medan, in 2012. Since 2015, she has been a Lecturer with the Department of Electrical Engineering Education and the Faculty of Education and Teacher Training, UIN Ar-Raniry Banda Aceh, Indonesia. Her research interests include renewable energies, automation and control systems, power electronics, and power quality.

YUWALDI AWAY (Member, IEEE) was born in South Aceh, Indonesia, in 1964. He received the degree in electrical-computer engineering from the Sepuluh Nopember Institute of Technology (ITS), Indonesia, in 1988, the M.Sc. degree from Bandung Institute of Technology (ITB), Indonesia, in 1993, and the Ph.D. degree in industrial computer from the National University of Malaysia (UKM), in 2000. Since 1990, he has been a Lecturer with the Department of Electrical and Computer Engineering, Faculty of Engineering, Universitas Syiah Kuala (USK), Indonesia. From 1996 to 2000, he was a Research Assistant with UKM, and from 2001 to 2004, he became a Lecturer. Since 2007, he has been a Professor and the Head of the Research Group for Automation and Robotics Studies, Syiah Kuala University. His research interests include combination of theory and practical, including microprocessor-based systems, simulation, automation, and optimization.

TARMIZI (Member, IEEE) was born in Pidie, Aceh, in January 1972. He received the degree from the Faculty of Engineering, Universitas Sumatera Utara, in 1998, and the master's and Ph.D. degrees from Universiti Sains Malaysia, in 2018. He has been a Lecturer with the Department of Electrical and Computer Engineering, Universitas Syiah Kuala (USK), since 1999. He was the Head of the Control System Laboratory and the Power Electronics Laboratory, Department of Electrical and Computer Engineering, USK, from 2000 to 2004 and from 2012 to 2015, respectively. He is currently the Head of the Department. His research interests include power converters for renewable energy and power quality.

IRA DEVI SARA (Member, IEEE) was born in Banda Aceh, Aceh, in May 1977. She received the master's degree in electrical engineering from Monash University, and the Ph.D. degree from Loughborough University, in 2014. Her master's project was the feasibility of integrating wind power systems with hydrogen storage for Victorian Coastal sites. Her Ph.D. project was the Polychromatic Determination of Spectral Response of Photovoltaic Devices. She is currently the Head of the Power Electronic and Renewable Energy Laboratory, Department of Electrical and Computer Engineering, Universitas Syiah Kuala (USK). Her research interests include the applied photovoltaic systems, power electronics, and renewable energies.

ROSLIDAR (Member, IEEE) received the bachelor's degree in electrical engineering from Universitas Syiah Kuala (USK), in 2002, the master's degree in telecommunication engineering from the University of Arkansas, USA, in 2009, and the Ph.D. degree, in January 2022. Since 2003, she has been a Lecturer with USK. She has been actively doing research in science and technology. She was a Visiting Scholar with the Faculty of System Design, Tokyo Metropolitan University, Japan, in May 2014. She dedicated her time to developing the e-health monitoring system using a non-invasive technique. She was granted a Fulbright Scholarship for the master's degree from the University of Arkansas.

ANDRI NOVANDRI (Student Member, IEEE) was born in Aek Kanopan, North Sumatra, in 1994. He received the Bachelor of Engineering degree in electrical and computer engineering from Universitas Syiah Kuala (USK), in 2017, and the Master of Engineering degree, in 2023. Since 2018, he has been a Research Assistant with USK, and has published several scientific articles. In 2024, he began teaching as a Lecturer with the Department of Computer Engineering, Faculty of Engineering, Universitas Serambi Mekkah (USM). His research interests include embedded systems, robotics, automation and control systems, sensors, and neural networks.

ANFIS_Parallelization_Control_on_Triple-Axis_Sun_Tracker_to_Minimize_Solar_Rays_Incidence_Angle_...

ORIGINALITY REPORT

7%	1%	6%	3%
SIMILARITY INDEX	INTERNET SOURCES	PUBLICATIONS	STUDENT PAPERS

PRIMARY SOURCES

1	AM Almas Shahriyar Azad, Khaled Mohammad Shifullah Bhuiya, Sumaiya Rashid Shoshi, Jubayer Rahman Jamal et al. "Harnessing the sun: Framework for development and performance evaluation of AI-driven solar tracker for optimal energy harvesting", Energy Conversion and Management: X, 2025 Publication	2%
2	Yuwaldi Away, Andri Novandri, Isyatur Raziah, Melinda Melinda. "A New Technique for Improving the Precision of Dual-Axis Tetrahedron-Based Sensor With Switching Between PID and ANN", IEEE Access, 2023 Publication	1%
3	Nazmul Siddique, Hojjat Adeli. "Computational Intelligence", Wiley, 2013 Publication	1%
4	Yuwaldi Away, Andri Novandri, Isyatur Raziah, Melinda. "A New Technique for Improving the Precision of Dual-axis Tetrahedron-based Sensor with Switching between PID and ANN", IEEE Access, 2023 Publication	1%
5	strathprints.strath.ac.uk Internet Source	1%
6	Submitted to Imperial College of Science, Technology and Medicine	1%

Student Paper

7	www.rairo-ro.org Internet Source	1 %
8	Submitted to University of Kufa Student Paper	1 %

Exclude quotes	Off	Exclude matches	< 1%
Exclude bibliography	On		